Asian Journal of Chemistry; Vol. 35, No. 4 (2023), 935-941

ASIAN JOURNAL OF CHEMISTRY

https://doi.org/10.14233/ajchem.2023.26949

A Study on Morphological Effect of Nano WO_3 Particles for Dye Sensitized Solar Cell Application

S. JAYAKUMAR[1,*] and J. POONGKOTHAI[2]

[1]Department of Physics, Chikkanna Government Arts College, Tiruppur-641602, India
[2]Department of Mathematics, Government Arts College, Udumalpet-642126, India

*Corresponding author: E-mail: sjayakumar.physics@gmail.com

Received: 6 November 2022; *Accepted*: 26 February 2023; *Published online*: 30 March 2023; AJC-21193

Tungsten oxide (WO_3) nanoparticles of rod-like and spherical morphologies were synthesized using sol-gel modified Pechini's method. The spherical morphology is achieved by optimizing precursor concentration. The synthesized WO_3 nanoparticles were characterized by powder XRD for phase analysis and SEM for size and morphological analysis. It was revealed that the synthesized particles have spherical and rod-like shapes, are in the monoclinic phase and in the nano range. Dye sensitized solar cells were fabricated by incorporating WO_3 nanoparticles in 0.5, 1 and 2 wt.% with anatase TiO_2 nanoparticles and their photovoltaic characteristics were investigated. It was found that the incorporation of WO_3 nanoparticles with nano TiO_2 particles considerably enhanced the short circuit current density (J_{sc}) and power conversion efficiency (η). Further, it was found that WO_3 nanoparticles with small size and spherical morphology have higher short circuit current density (13.27 mA cm^{-2}) and power conversion efficiency (6.63%) compared to rod-like WO_3 nanoparticles.

Keywords: WO_3 nanoparticles, Dye sensitized solar cell, Photovoltaic cells, Sol-gel method, Pechini's method.

INTRODUCTION

Photovoltaic cells becoming the most promising source of sustainable energy supplier because of their low manufacturing cost, simple structure, abundance of material and reasonable efficiency. Among this category, dye sensitized solar cells (DSSCs) are being extensively investigated for future generation energy converters due to their energy conversion efficiency and compactness [1]. The energy conversion efficiency of a DSSC can be improved by adopting a suitable photosensitizer (dye), increasing light harvesting efficiency and minimizing photogenerated electron-hole pair recombination rate. Dye sensitizers are used to stimulate photocatalytic reactions over the surface of wide band gap semiconductors (WBGS) like ZnO, TiO_2 *etc.*, which are commonly used as photoanode material [2].

Optimal DSSC performance can also be enhanced by selecting the photoanode material. TiO_2 is a visibly transparent, wide band gap semiconductor (3.2 eV), which does not suppress the light absorbing efficiency of the dye sensitizers. The structural arrangement of its conduction band (CB) favours good open-circuit voltage and electron injection from the excited dyes [3]. TiO_2 exhibits good stability under the exposure of most of the corrosive acids. Further, TiO_2 nanoparticles offer enhanced surface to volume ratio, which is the crucial for maximum light absorption. TiO_2 in nano regime finds applications in area of sensing, water purification, agricultural and medical industry in addition to solar energy harvesting [4].

Meen *et al.* [5] developed a DSSC using nano TiO_2 synthesized by spin coating and obtained power conversion efficiency of 1.95%. The enhancement is attributed to the improved visible light absorption characteristics and ability to transfer the photogenerated electrons from the sensitizer to the conduction band of TiO_2 [5]. It was also demonstrated that the electron injection capacity could be increased and recombination rate could be reduced when benzyl alcohol synthesized Nb:TiO_2 is surface treated with $TiCl_4$ [6].

One dimensional nano-TiO_2 structures such as nano wires, nano rods and nano tubes are also demonstrated as candidate for photoanode material due to their higher electron transport and light scattering capability [7-9]. Jennings *et al.* [10] reported that when ordered array of TiO_2 nanotubes were used in photoanodes, an ideal electron collection efficiency could be achieved [10]. Maheswari & Sreenivasan [11] reported that when nano-TiO_2 are used in the form of core-shell structures

or bilayers inhibition of recombination of photo generated charge carriers occur effectively [11]. Nano-TiO_2 particle/TiO_2 fiber composite as photoanode found to be exhibit an improved light harvesting ability and hence enhanced efficiency [12].

Zheng *et al.* [13] used porous WO_3 thin film as photoanode material for DSSC and found that its efficiency could be improved to 1.46% when the photoanode was treated with $TiCl_4$. When nano-WO_3 with oxygen vacancies are used as counter electrode material, the efficiency of DSSC was found to increase considerably due to enhanced electrical conductivity [14]. Further, WO_3 nanotubes are reported to exhibit better electron injection from the dye to electrode particularly when dyes having very positive LUMO levels are used as sensitizer [15]. Habibi *et al.* [16] hydrothermally synthesized nano-WO_3 particles and fabricated photoanode for DSSC, which demonstrated a power conversion efficiency of 4.1% [16].

Tungeston oxide (WO_3) nanoparticles have been synthesized by variety of methods including solvothermal, hydrothermal and plasma processing method [17]. To improve the overall performance of DSSC, recently, photoanodes are being fabricated by more than one material. This approach attracts the attention of researchers because it is possible to combine the obvious advantages of different materials. TiO_2/ZnO nano composites have also been investigated many researchers to ease the process of charge carrier separation and inhibit their recombination [18-20]. The present work demonstrates synthesis of WO_3 nanoparticles of rod-like and spherical morphology using sol-gel modified Pechini's method and fabrication of photoanode using WO_3 nanoparticles and reactive plasma synthesized TiO_2 nanoparticles. Reactive plasma processing takes the advantage of the high temperature and high enthalpy of the thermal plasma jet to effect 'in-flight' chemical reactions in the presence of a reactive gas to synthesize nano-sized powders of advanced ceramics, novel coatings and convert minerals and industrial wastes to value added material [21]. The effect of adding WO_3 nanoparticles and its morphology on the performance of the DSSC has been presented.

EXPERIMENTAL

Sodium tungstate dihydrate ($Na_2WO_4{\cdot}2H_2O$, 99.99%, Sigma-Aldrich) powder, hydrochloric acid (37%, Sigma-Aldrich) and nitric acid (68%, Sigma Aldrich) were used for ion-exchange reaction. Oxalic acid dihydrate powder ($H_2C_2O_4{\cdot}2H_2O$, 99.99%, Sigma-Aldrich) and polyethylene glycol (PEG 200, 99.99%, Sigma Aldrich) were used as the complexing agent and polymeric source, respectively.

Synthesis: $Na_2WO_4{\cdot}2H_2O$ powder (12 mmol) was dissolved in water and then heated at 80 ºC. Then, a mixture of HCl and HNO_3 (molar ratio of 1:1) was added to the solution at the same temperature, while it was being stirred, to adjust the pH to 1-2 and enhance ion-exchange process. After a while, the yellow precipitate was formed and converted into a soft gel through aging. Then the gel was washed by the addition of hot distilled water to gel followed by stirring and aging the soft gel at the same temperature. The product was washed several times to remove the residual acid and byproducts. Oxalic acid (32 mmol) and PEG 200 (1 mmol) were then added as chelating and resin agents, respectively. Finally, the WO_3 nanoparticles were synthesized by heat treatment of resin precursor prepared from the hydrated tungstic precipitates. The samples were first heated at 150 ºC to remove residual water, then heated to 550 ºC and kept at this temperature for 90 min followed by cooling to room temperature. Similarly, another sample was prepared using 50 mmol $Na_2WO_4{\cdot}2H_2O$, 260 mmol oxalic acid and 8 mmol PEG and named as sample 2. The nano-TiO_2 powder has been synthesized from micron size TiH_2 powder by reactive plasma processing and used to prepare TiO_2 photoanode [22].

To study the effect of incorporation of WO_3 nanoparticles in TiO_2 photoanode systematically, photoanodes were fabricated with incorporation of WO_3 nanoparticles in different ratio (0, 0.5, 1.0 and 2.0 wt.%). For the fabrication of 1% WO_3 incorporated photoanode, a mixture containing (0.1 g WO_3 + 2.0 g TiO_2) + 5.0 g α-terpineol + 0.5 g cellulose + 20 mL ethanol) was prepared and solicited for 30 h at 1200 W cm^{-2}. The prepared paste was coated on a FTO conducting glass plate using the doctor blade technique. This thin film was annealed at 350 ºC for 20 min. In next step, the prepared thin film electrode was immersed in a dye solution (N719) of concentration (0.0004 M) at room temperature for 30 h, rinsed with anhydrous ethanol and dried. Similarly, FTO conducting glass plate coated with platinum was then placed above the prepared electrode and the sides of the prepared dye sensitized solar cell was tightly covered with the sealing sheet (PECHM-1). A mixture of the (0.5 M KI + 0.05 M I2 + 0.5 M 4-*tert*-butylpyridine) was used as redox electrolyte. Similarly, DSSCs with different percentages (0, 0.5, 1.0 and 2.0 wt.%) of samples 1 and 2 were fabricated. A schematic of WO_3 incorporated TiO_2 dye sensitized solar cell representation is shown in Fig. 1.

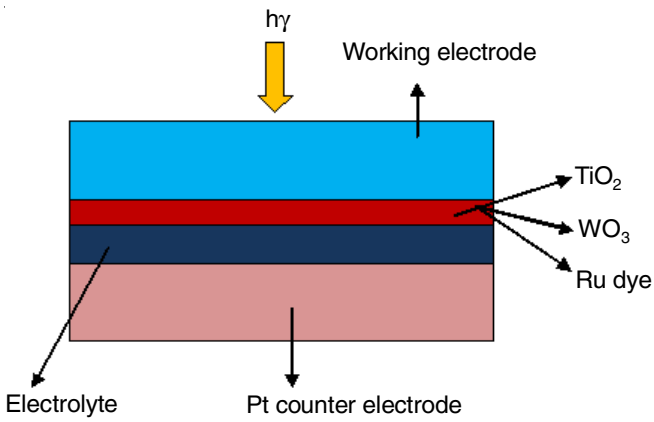

Fig. 1. Schematic representation of WO_3 incorporated TiO_2 dye sensitized solar cell

Characterization: The X-ray diffraction (XRD) patterns were recorded using a Bruker D8 Advance diffractometer equipped with Ni filter and operated at 40 kV, 30 mA (Cu $K\alpha_1$ radiation). Particle size and morphology of the samples were carried out using JSM-35CF scanning electron microscope and JEOL transmission electron microscope (JEM 2100F, Japan) operated at 200 KV. The UV visible spectrum of the sample was obtained using a Shimatzo's UV visible spectrophotometer-1800. The current and voltage (I-V) characteristics were

measured used the white light from a xenon lamp (λ_{max} = 150 W) used as a sun of 2000 solar simulator. Light intensity was adjusted used in a Si solar cell to ~AM-1.5, when the incident light intensity and the active cell area was 100 mW cm^{-2} (one sun illumination) amd 0.25 cm^2 (0.5 × 0.5 cm), respectively.

RESULTS AND DISCUSSION

XRD studies: The X-ray diffraction patterns of sol-gel modified Pechini's method synthesized nano-WO_3 particles is shown in Fig. 2. The obtained XRD patterns confirmed the formation of pure monoclinicWO_3 crystalline phase as per JCPDS file no. 43-1035 [23]. The intensities of both powders depicted the good crystallinity of WO_3 nanopowders. The crystallite sizes of both the samples 1 and 2 were determined using Schererr's formula:

$$D = \frac{0.9\lambda}{\beta \cos\theta}$$

where D is crystallite size (nm), λ is the wavelength of X-ray radiation, θ is the Bragg's angle and β is the full width half maximum (FWHM)) [24]. The crystallite size for samples 1 and 2 was found to be 70 nm and 42 nm, respectively.

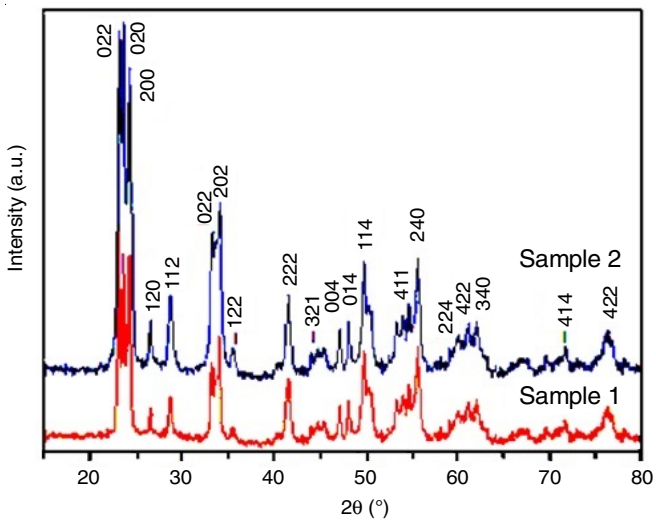

Fig. 2. X-ray diffraction patterns of sol-gel modified Pechini's method synthesized nano WO_3 particles

Morphological studies: The FE-SEM images of samples 1 and 2 are shown in Fig. 3. Fig. 3a shows the SEM image of sample 1, which displays mixture of the rod-like and elongated

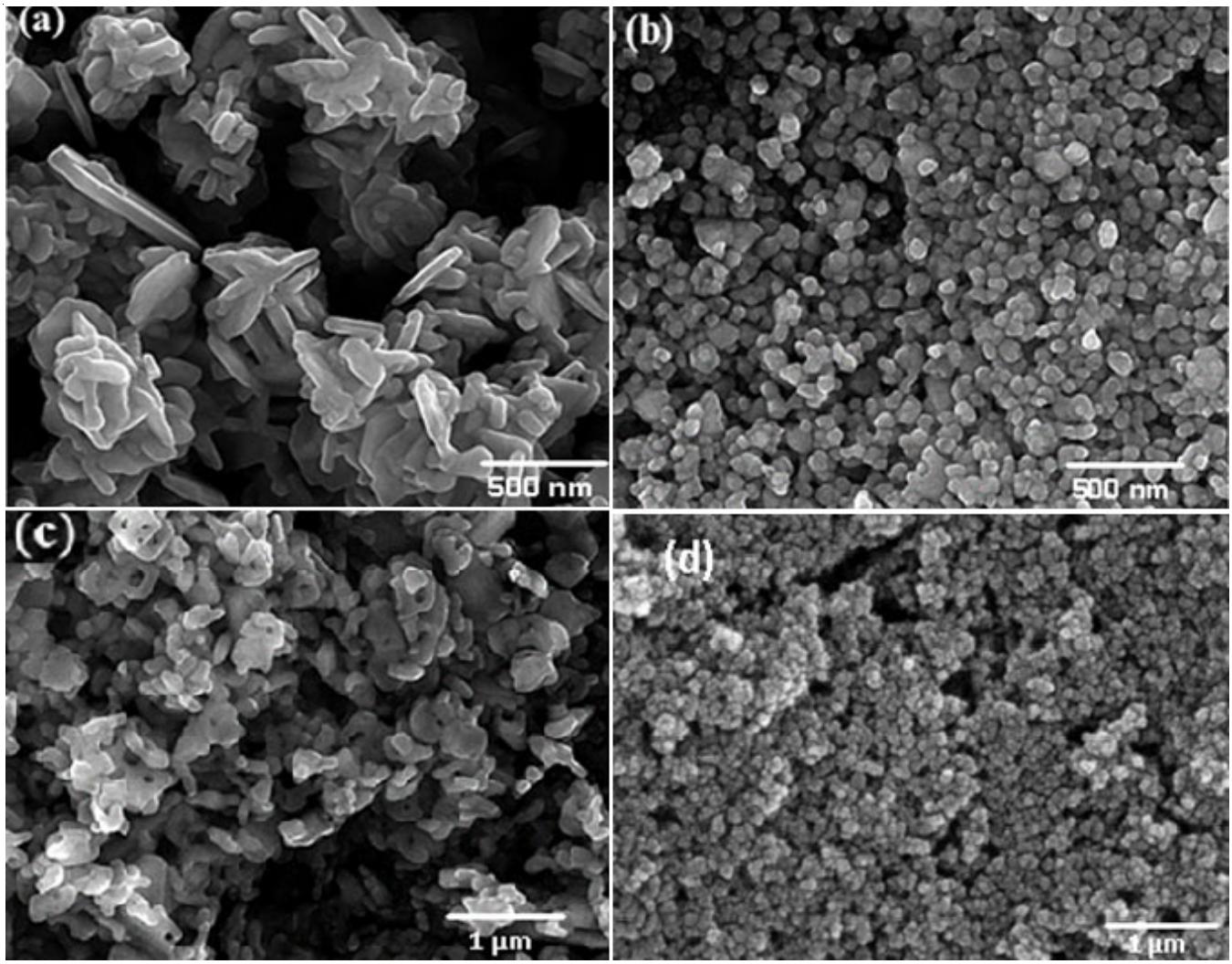

Fig. 3. FE-SEM images of sol-gel modified pechini's method synthesized nano WO_3 particles: (a), (c) sample 1, (b), (d) sample 2

sphere WO_3 particles. The average thickness of the particle is calculated to be 75 nm. But the length of particle varies from 150 nm to 300 nm and few particles with length greater than 500 nm. The formation of rod-like morphology is attributed to the minimum amount of chelating agent (32 mmol) and PEG (1 mmol). Fig. 3a shows the SEM image of sample 2, which displays the spherical shape particles with a uniform size distribution. The average particle size was found to be 45 nm. The formation of uniform spherical morphology is attributed to the higher amount of chelating agent (260 mmol) and PEG (8 mmol).

Fig. 4 shows the transmission electron microscopic images of sol-gel modified Pechini's method synthesized nano-WO_3 particles. The TEM image of sample 1 (Fig. 4a) clearly shows the rod-like and elongated spherical particles of length greater than 150 nm, whereas the TEM image shown in Fig. 4b clearly reveals the spherical morphology of the synthesized nano-WO_3 particles. It was observed that most of the particles are below 50 nm size except few of size above 50 nm.

The TEM image and XRD pattern of reactive plasma synthesized TiO_2 nanoparticle is shown in Fig. 5. TEM image (Fig. 3a) clearly shows that the particles are having spherical morphology and size varies from 10-50 nm. The XRD pattern reveals that the reactive plasma synthesized TiO_2 nanoparticles are mixture of anatase and rutile phase.

UV-visible studies: The UV-visible absorption spectrum of the sol-gel modified Pechini's method synthesized nano-WO_3 particles is shown in Fig. 6. The nano-WO_3 particles having broad absorption band with maxima at 345 nm. The effect of reduced size of WO_3 particles causes the absorption edge to shift slightly to red, from 473 nm in sample 1 to 503 nm in sample 2 [25].

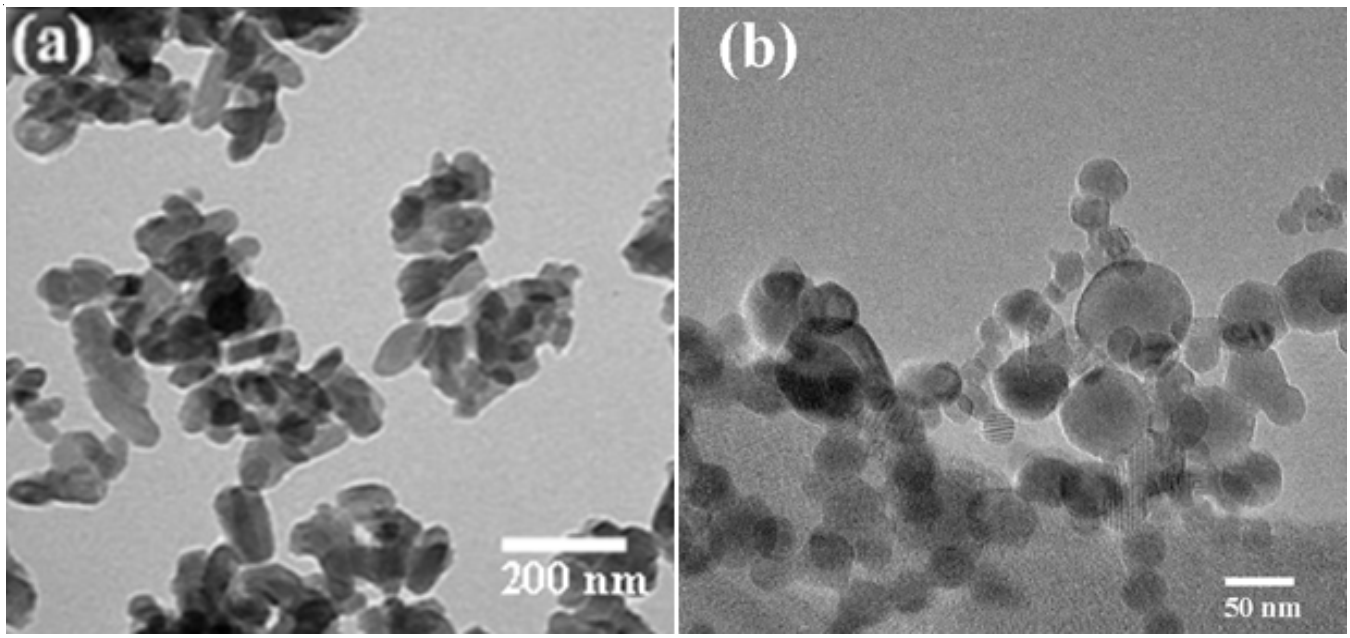

Fig. 4. TEM images of sol-gel modified Pechini's method synthesized nano WO_3 particles: (a) sample 1, (b) sample 2

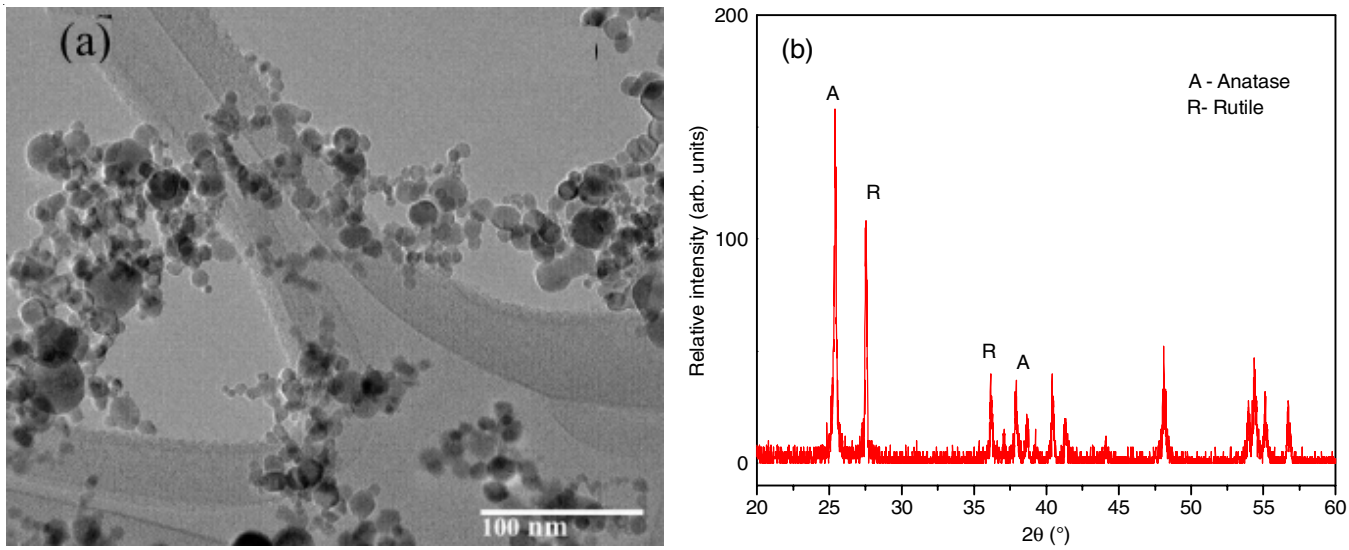

Fig. 5. Reactive plasma synthesized TiO_2 particle: (a) TEM image and (b) XRD pattern

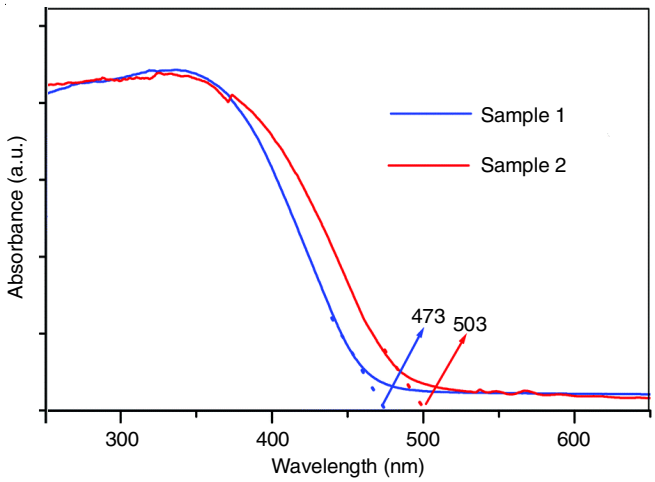

Fig. 6. UV-visible absorption spectrum of the sol-gel modified Pechini's method synthesized nano WO_3 particles

The fabricated DSSCs are subjected to photovoltaic investigation and the results are discussed. Fig. 7a shows the J-V characteristics of DSSCs prepared with pure TiO_2 nanoparticles, 0.5% WO_3 (sample 1) with TiO_2 nanoparticles, 1% WO_3 (sample 1) with TiO_2 nanoparticles and 2% WO_3 (sample 1) with TiO_2 nanoparticles. From the J-V curve, the short circuit current density (J_{sc}), open circuit voltage (V_{oc}), power conversion efficiency (η) and fill factor (FF), for the dye sensitized solar cell (DSSC) prepared using pure TiO_2 as a photoanode material, were determined to be 6.32 mA cm^{-2}, 0.612 V, 2.54% and 0.657, respectively. Similarly, for a DSSC prepared with 0.5% rod-like WO_3 nanoparticles (sample 1) as photoanode material, the short circuit current density (J_{sc}), open circuit voltage (V_{oc}), power conversion efficiency (η) and fill factor (FF) were calculated to be 12.51 mA cm^{-2}, 0.678 V, 5.596% and 0.698, respectively. The short circuit current density (J_{sc}), open circuit voltage (V_{oc}), power conversion efficiency (η) and fill factor (FF), for TiO_2 with 1% rod-like WO_3 nanoparticles (sample 1) as photoanode material, were determined to be 12.92 mA cm^{-2}, 0.689 V, 6.2126% and 0.6979, respectively. When the nano-WO_3 was increased to 2%, short circuit current density (J_{sc}), open circuit voltage (V_{oc}), power conversion efficiency (η) and fill factor (FF) were determined to be 11.73 mA cm^{-2}, 0.661 V, 5.0925% and 0.6568%, respectively.

Fig. 6b shows the J-V characteristics of DSSCs prepared with pure TiO_2 nanoparticles, 0.5% WO_3 (sample 2) with TiO_2 nanoparticles, 1% WO_3 (sample 2) with TiO_2 nanoparticles and 2% WO_3 (sample 2) with TiO_2 nanoparticles. From the J-V curve, short circuit current density (J_{sc}), open circuit voltage (V_{oc}), power conversion efficiency (η) and fill factor (FF), for the dye sensitized solar cell (DSSC) prepared using pure TiO_2 with 0.5% spherical WO_3 nanoparticles (sample 2) as photo anode material, are determined to be 12.78 mA cm^{-2}, 0.71 V, 5.9161% and 0.6752, respectively. Similarly, for a DSSC prepared with 1% spherical WO_3 nanoparticles (sample 2) as photoanode material, the short circuit current density (J_{sc}), open circuit voltage (V_{oc}), power conversion efficiency (η) and fill factor (FF) were calculated to be 13.27 mA cm^{-2}, 0.713 V, 6.6334% and 0.7011% respectively. When the nano-WO_3 was increased to 2%, the corresponding short circuit current density (J_{sc}), open circuit voltage (V_{oc}), power conversion efficiency (η) and fill factor (FF) were determined to be 12.11 mA cm^{-2}, 0.615 V, 4.938% and 0.6631, respectively. The photovoltaic parameters of the DSSCs prepared using WO_3 nanoparticles are displayed in Table-1.

From the above observation, it is found that the short circuit current density is increased in WO_3 incorporated DSSCs in comparison to pure TiO_2 DSSCs. This increase in short circuit current density is attributed due to the addition of WO_3 nanoparicles, which enhances the process of adsorbing of dye molecules. This in turn enhances photon absorbing capacity and hence injects the photogenerated electrons to the conduction band to generate current. However, when nano-WO_3 addition is increased to 2%, the short circuit current density and open circuit voltage decreases and results decrease in power conversion efficiency irrespective of particle morphology. Compared to

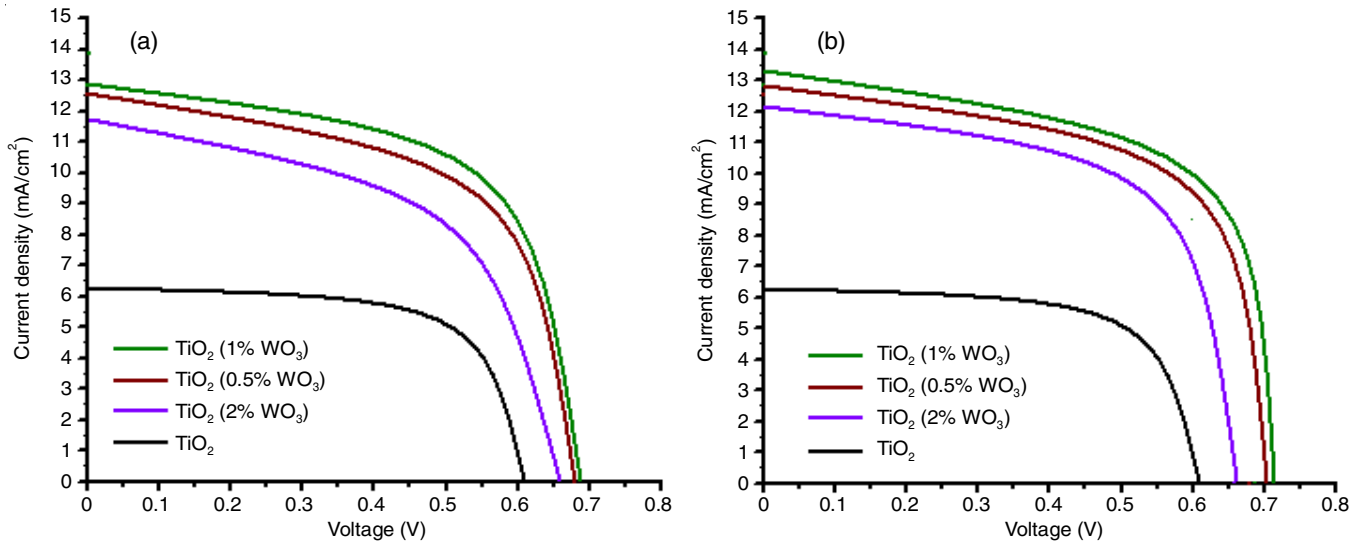

Fig. 7. J-V characteristics of DSSCs developed using different percentages of WO_3 nanoparticles and the incident photon-to-current conversion efficiency

TABLE-1
PHOTOVOLTAIC PARAMETERS OF THE DSSCs PREPARED USING WO_3 NANOPARTICLES

Photo anode material	Nano WO_3 content (%)	J_{sc} (mA cm^{-2})	V_{oc} (V)	FF	η (%)
Pure TiO_2	0	6.32	0.612	0.6578	2.5400
TiO_2 + Sample 1 (Rod-like WO_3)	0.5	12.51	0.678	0.6598	5.5962
	1	12.92	0.689	0.6979	6.2126
	2	11.73	0.661	0.6568	5.0925
TiO_2 + Sample 2 (spherical WO_3)	0.5	12.78	0.710	0.6752	5.9161
	1	13.32	0.713	0.7011	6.6334
	2	12.11	0.615	0.6631	4.9380

0.5% and 1% addition, 2% nano-WO_3 added DSSC exhibited lower short circuit current density and power conversion efficiency (both samples 1 and 2).

Possible reasons for the observed decrease in short circuit current density (J_{sc}) for 2% addition of WO_3 nanoparticles can be listed as follows. At increased concentration of WO_3 nanoparticles, the presence of surplus amount of WO_3 nanoparticles on the surface results unproductive gathering of the photo-injected electrons. The surplus nanoparticles may possibly, further increase the series resistance between the FTO and TiO_2 nanoparticle structures. Further, the reduced dye adsorption area and higher possibility for charge recombination are also the reasons for the reduction of power conversion efficiency [26].

Furthermore, the morphology of nano-WO_3 particles incorporated as a photoanode material has considerable effect on the short circuit current density (J_{sc}) and power conversion efficiency. The nano-WO_3 particles with spherical morphology (sample 2) have higher short circuit current density (J_{sc}) and power conversion efficiency for 0.5%, 1% and 2% addition compared with rod-like morphology (sample 2). This higher current conversion efficiency is possible attributed to spherical morphology and small particle size, which offers the high surface area for adsorbing dye molecules that acts as enhanced photo-receiver.

Conclusion

Tungsten oxide (WO_3) nanoparticles with rod-like and spherical morphologies were synthesized using sol-gel modified Pechini's method. The morphology of the synthesized nanoparticles were characterized by X-ray powder diffraction and scanning electron microscopy. By using the synthesized WO_3 nanoparticles (0%, 0.5%, 1% and 2% addition) dye sensitized solar cells were fabricated. It is primarily found that the incorporation of WO_3 nanoparticles with reactive plasma synthesized TiO_2 particles considerably enhanced the short circuit current density (J_{sc}) and power conversion efficiency (η). Further, it found that the spherical WO_3 nanoparticles demonstrated higher short circuit current density and power conversion efficiency for concentrations of WO_3 nanoparticles compared to rod-like particles. A higher short circuit current density (13.32 mA cm^{-2}) and power conversion efficiency (6.6334%) was achieved for spherical WO_3 nanoparticles with 1% addition.

ACKNOWLEDGEMENTS

The authors thank to Plasma Spray Technologies Section, Laser and Plasma Technology Development Division, BARC, Mumbai, India for permitting to carry out experimental works and avail the laboratory facilities.

CONFLICT OF INTEREST

The authors declare that there is no conflict of interests regarding the publication of this article.

REFERENCES

1. C.P. Lee, C.T. Li and K.C. Ho, *Mater. Today*, **20**, 267 (2017); https://doi.org/10.1016/j.mattod.2017.01.012
2. X. Zhang, T. Peng and S. Song, *J. Mater. Chem. A Mater. Energy Sustain.*, **4**, 2365 (2016); https://doi.org/10.1039/C5TA08939E
3. M. Baraton, *Recent Pat. Nanotechnol.*, **6**, 10 (2012); https://doi.org/10.2174/187221012798109273
4. R. Rathinam, D.P. Singh, A. Dutta, S. Rudresha, S.R. Ali and P. Chatterjee, *Adv. Sci. Technol.*, **117**, 85 (2022); https://doi.org/10.4028/p-7in58j
5. T.H. Meen, W. Water, W.R. Chen, S.M. Chao, L.W. Ji and C.J. Huang, *J. Phys. Chem. Solids*, **70**, 472 (2009); https://doi.org/10.1016/j.jpcs.2008.12.002
6. M. Stefik, F.J. Heiligtag, M. Niederberger and M. Grätzel, *ACS Nano*, **7**, 8981 (2013); https://doi.org/10.1021/nn403500g
7. M. Adachi, Y. Murata, J. Takao, J. Jiu, M. Sakamoto and F. Wang, *J. Am. Chem. Soc.*, **126**, 14943 (2004); https://doi.org/10.1021/ja048068s
8. B.H. Lee, M.Y. Song, S.Y. Jang, S.M. Jo, S.Y. Kwak and D.Y. Kim, *J. Phys. Chem. C*, **113**, 21453 (2009); https://doi.org/10.1021/jp907855x
9. C.J. Lin, W.Y. Yu and S.H. Chien, *J. Mater. Chem.*, **20**, 1073 (2010); https://doi.org/10.1039/B917886D
10. J.R. Jennings, A. Ghicov, L.M. Peter, P. Schmuki and A.B. Walker, *J. Am. Chem. Soc.*, **130**, 13364 (2008); https://doi.org/10.1021/ja804852z
11. D. Maheswari and D. Sreenivasan, *Appl. Sol. Energy*, **51**, 112 (2015); https://doi.org/10.3103/S0003701X15020085
12. P. Joshi, L. Zhang, D. Davoux, Z. Zhu, D. Galipeau, H. Fong and Q. Qiao, *Energy Environ. Sci.*, **3**, 1507 (2010); https://doi.org/10.1039/c0ee00068j
13. H. Zheng, Y. Tachibana and K. Kalantar-zadeh, *Langmuir*, **26**, 19148 (2010); https://doi.org/10.1021/la103692y
14. L. Cheng, Y. Hou, B. Zhang, S. Yang, J.W. Guo, L. Wu and H.G. Yang, *Chem. Commun.*, **49**, 5945 (2013); https://doi.org/10.1039/c3cc42206b
15. K. Hara, Z. Zhao, Y. Cui, M. Miyauchi, M. Miyashita and S. Mori, *Langmuir*, **27**, 12730 (2011); https://doi.org/10.1021/la201639f
16. M.H. Habibi, M. Mikhak, M. Zendehdel and M. Habibi, *Int. J. Electrochem. Sci.*, **7**, 6787 (2012).
17. N. Prabhu, S. Agilan, N. Muthukumarasamy and T.S. Senthil, *J. Mater. Sci. Mater. Electron.*, **25**, 5288 (2014); https://doi.org/10.1007/s10854-014-2303-6

18. N. Sakai, T. Miyasaka and T.N. Murakami, *J. Phys. Chem. C*, **117**, 10949 (2013); https://doi.org/10.1021/jp401106u
19. S.S. Kim, J.H. Yum and Y.E. Sung, *J. Photochem. Photobiol. Chem.*, **171**, 269 (2005); https://doi.org/10.1016/j.jphotochem.2004.10.019
20. C.S. Chou, F.C. Chou and J.Y. Kang, *Powder Technol.*, **215–216**, 38 (2012); https://doi.org/10.1016/j.powtec.2011.09.003
21. S. Jayakumar, P.V. Ananthapadmanabhan, T.K. Thiyagarajan, K. Perumal, S.C. Mishra, G. Suresh, L.T. Su and A.I.Y. Tok, *Mater. Chem. Phys.*, **140**, 176 (2013); https://doi.org/10.1016/j.matchemphys.2013.03.018
22. S. Jayakumar, T.K. Thiyagarajan, P.V. Ananthapadmanabhan, K.P. Sreekumar, K. Perumal, S.C. Mishra, L.T. Su, A.I.Y. Tok, A.B. Garg, R. Mittal and R. Mukhopadhyay, *AIP Conf. Proc.*, **1349**, 257 (2011); https://doi.org/10.1063/1.3605832
23. B. Yang, Y. Zhang, E. Drabarek, P.R.F. Barnes and V. Luca, *Chem. Mater.*, **19**, 5664 (2007); https://doi.org/10.1021/cm071603d
24. L.F. Reyes, S. Saukko, A. Hoel, V. Lantto and C.G. Granqvist, *J. Eur. Ceram. Soc.*, **24**, 1415 (2004); https://doi.org/10.1016/S0955-2219(03)00417-5
25. C.L. Veenas, L.R. Asitha, V.C. Bose, A.S. Aiswarya Raj, G. Madhu and V. Biju, *IOP Conf. Series: Mater. Sci. Eng.*, **73**, 012119 (2015); https://doi.org/10.1088/1757-899X/73/1/012119
26. H.H.T. Vu, Y.H. Hwang and H.K. Kim, *Curr. Photovoltaic Res.*, **4**, 42 (2016); https://doi.org/10.21218/CPR.2016.4.2.042